Colloids and Surfaces A: Physicochemical and Engineering Aspects 742 (2026) 140415

Contents lists available at ScienceDirect

Colloids and Surfaces A: Physicochemical and Engineering Aspects

journal homepage: www.elsevier.com/locate/colsurfa

# Rheological characterization of solid lipids with domain structure

A. Todorova, D. Cholakova, N. Denkov, S. Tcholakova *

*Department of Chemical and Pharmaceutical Engineering, Faculty of Chemistry and Pharmacy, Sofia University, 1 James Bourchier Avenue, Sofia 1164, Bulgaria*

## HIGHLIGHTS

- Visco-elasto-plasticity of alkane rotator phases are studied via SR and CR rheological tests.
- A generalized Kelvin-Voigt model accurately describes the observed behavior.
- Three distinct relaxation process are identified, $t_1 \approx 0.45$ s, $t_2 \approx 8$–$9$ s, $t_3 \approx 140 - 200$ s.
- A molecular interpretation of the relaxation mechanisms is proposed.
- A framework linking rheology to molecular dynamics in polycrystalline materials is proposed.

## GRAPHICAL ABSTRACT

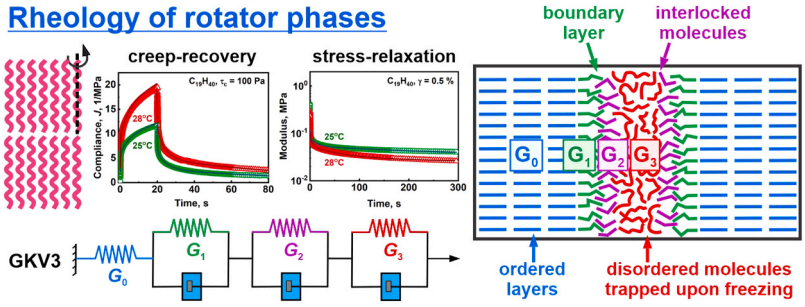


## ARTICLE INFO

*Keywords:*
Rheology
Stress-relaxation
Creep-recovery
Crystallization
Oil
Freezing
Alkane

## ABSTRACT

Phase behavior of lipids is of primary importance for the manufacturing and applications of foods, cosmetics and pharmaceuticals, as well as for the functions of biological membranes. Upon cooling, the molten bulk lipids crystallize into ordered domains which determine their rheological properties. While storage and loss moduli are typically used to describe these properties, their direct connection to the underlying molecular rearrangement remains poorly understood. In the current study, we performed a detailed rheological characterization of the rotator phases (intermediate phases between fully ordered crystalline and completely disordered liquid phases) formed in bulk linear alkanes. Large series of stress-relaxation and creep-recovery experiments were performed and interpreted, using generalized Kelvin-Voigt model with one spring, connected in series with three combined elements of a spring and a dashpot. We determined the elasticities and viscosities of all these rheological elements, along with the respective three relaxation times of the combined elements. These relaxation times are governed by different molecular processes in the sheared samples and differ by three orders of magnitude: $t_1 \approx 0.45$ s and $t_2 \approx 8$–$9$ s are related to local molecular rearrangements at the domain boundaries, while $t_3 \approx 140$–$200$ s most probably describes the rearrangement of disordered lipid molecules entrapped between the ordered domains. The storage and loss moduli, calculated from the constants of the generalized Kelvin-Voigt model, were in a very good agreement with those measured directly in amplitude sweep and temperature ramps oscillatory tests, thus supporting the self-consistency of data interpretation. The methodology presented here is applicable to other polycrystalline lipid materials with 2D or 3D domain structures, providing a valuable framework for interpreting their rheological behavior.

* Corresponding author.
*E-mail address:* sc@lcpe.uni-sofia.bg (S. Tcholakova).

https://doi.org/10.1016/j.colsurfa.2026.140415
Received 28 January 2026; Received in revised form 17 March 2026; Accepted 31 March 2026
Available online 1 April 2026

## 1. Introduction

Crystals formed from hydrophobic molecules (generally referred to as lipids) often determine the texture, spreadability, and overall appearance of various everyday products. These include foods such as butter, ice cream, spreads and chocolate [1–6]; cosmetic products such as lip balms, creams and lotions [7–9], and many others. The phase behavior of lipids has also significant implications in biological systems, influencing critical processes such as the permeability of lipid membranes in the living cell [10], the wettability of insects [11], the self-healing ability of the plants [12,13], *etc*. In industrial applications, lipids are utilized in phase change materials (PCMs) for thermal storage [14–16].

Rotator phases (denoted as *R*) are intermediate phases found in alkanes (denoted hereafter as $C_n$), alkenes, long chain alcohols and other linear hydrophobic molecules. These phases exist between the fully disordered liquid phase and the highly ordered crystalline phase [13, 17–21]. In the rotator phase, molecules arrange in layered structures resembling crystals but lack a long-range positional order with respect to their rotational degree of freedom. The term "rotator phase" was introduced by Müller in 1932 [22] to highlight the partial rotational freedom around the molecular axis. Although rotator phases are intermediate between the liquid and solid states, their structural and mechanical properties closely resemble those of solid phases. This is underscored by the enthalpy released during the liquid-to-rotator phase transition, which typically accounts for *ca.* 75–80% of the total enthalpy associated with the liquid-to-crystal phase transition [17,23].

The rheological properties of rotator phases have significant practical implications. For example, the spreadability of cosmetic products, such as paraffin waxes and petroleum jelly, depends on the rheology of the underlying rotator structures [24,25]; the flowability of the phase-change materials (PCM) dispersions used in energy storage and transportation, and in air-conditioning installations [14,26]; as well as for various biological processes [17]. Despite this importance, the rheology of rotator phases has remained largely unexplored due to challenges in selecting suitable characterization methods and data interpretation approaches.

In a recent study, we developed a procedure for characterization of the rheological properties of rotator and crystalline phases formed by cooled lipids – long chain alkanes, alkenes or their mixtures [27]. Shear oscillatory experiments were performed upon cooling and heating with a constant rate at a fixed strain of $\gamma = 0.05\%$ and frequency $\nu = 1$ Hz. The results from this study showed that the rotator and crystalline phases of alkanes possess viscoelastic behavior with storage modulus being about one order of magnitude higher than the loss modulus. This is illustrated in Supplementary Figure S1 for nonadecane ($C_{19}$) where newly obtained data using the same experimental procedure as in Ref. [27] are shown. The shear storage modulus for rotator phases was $G' \approx 1\text{–}3 \times 10^5$ Pa, whereas the shear loss modulus was found to be $G'' \approx 3\text{–}9 \times 10^4$ Pa. After the rotator-to-crystalline phase transition took place, these moduli increased *ca.* 10 times, showing that the crystalline phase (*C*) is much stiffer compared to the rotator phase. For comparison, the same moduli for the liquid phase are negligible ($< 1$ Pa).

A slight temperature dependence of the storage and loss moduli was observed in our previous study [27] for both the rotator and crystalline phases, with moduli increasing as the temperature decreased, due to reduced molecular thermal energy and tighter molecular packing. In crystalline phases, the moduli exhibited linear relationships with subcooling that were independent of the lattice type, indicating that neither the unit cell structure nor the alkane length affects the crystalline phase shear rheology. In contrast, the moduli of the rotator phase decreased with increasing the chain length, which was attributed to the larger fraction of non-planar conformers present in longer alkanes [27]. These conformational defects are largely eliminated upon crystallization [28], which explained the universal temperature dependence observed for crystalline phase moduli of $C_{19}$-$C_{28}$ alkanes.

The aim of the present study is to deepen our understanding of the rheological behavior of linear alkanes in rotator phases and to identify the simplest rheological model, capable of accurately describing the observed visco-elasto-plastic response. In addition, we suggest a relation between the model parameters to the underlying molecular processes, thereby providing a physical interpretation of the observed macroscopic behavior. This approach is expected to be general and applicable for the description of various lipid systems with domain structure.

## 2. Materials and experimental methods

### 2.1. Materials

Two linear long-chain alkanes were studied – nonadecane ($C_{19}H_{40}$, denoted as $C_{19}$) and octacosane ($C_{28}H_{58}$, denoted as $C_{28}$). The alkanes used in the experiments had purity $> 99\%$ and were purchased by TCI ($C_{19}$) and Sigma-Aldrich ($C_{28}$). These alkanes were chosen because they have relatively wide temperature interval in which the rotator phases are stable, viz. between their crystal-to-rotator phase transition temperature, $T_{CR}$, and melting temperature, $T_{RL} \equiv T_m$. For nonadecane, $T_{CR} \approx 21.7°C$ and $T_{RL} \approx 32.0°C$, and for octacosane: $T_{CR} \approx 57.8°C$ and $T_{RL} \approx 61.3°C$, measured upon heating of the investigated alkanes. Note that these temperatures are slightly lower when measured upon cooling due to the subcooling phenomenon, viz. the rotator phase exists between ca. 21°C and 30°C for $C_{19}$, and from 56°C to 60°C for $C_{28}$, see Supplementary Figure S2.

### 2.2. Experimental methods

Rheological measurements were carried out to characterize the properties of the rotator phases for both alkanes. They were performed on rotational rheometers Discovery Hybrid Rheometer DHR-3 and HR-20 (TA Instruments, USA). Parallel plate geometry was used where the upper plate had a diameter of 40 mm and the gap between the two plates was set to 300 μm. To avoid potential wall slip, ultra-fine sandpaper of grade P1500 was glued to both plates before the experiment. Note that the obtained experimental results are for samples that are in the rotator phase. Within the selected temperature range, the studied rotator phases do not undergo a phase transition to the crystalline phase.

Prior to all measurements, the examined sample was loaded in a molten state (35°C for $C_{19}$ and 65°C for $C_{28}$), equilibrated at this high temperature for a period of 2 min and then cooled to the desired low temperature with a constant cooling rate. Rate of 2 °C/min was used for $C_{19}$ samples and 1 °C/min cooling was applied for $C_{28}$. We note that in a preliminary series of experiments, we also tested $C_{19}$ rotator phases prepared at 1 °C/min cooling, but no any difference was observed between the measurements performed with samples cooled at 1 and 2 °C/min, thus we continued with the higher cooling rate to optimize the time needed for this experimental step. Once the desired temperature was achieved, the temperature of the sample was equilibrated for 1 min before the subsequent rheological measurements were performed.

Two types of relaxation tests were performed – *creep-recovery* and *stress-relaxation*. During the *creep-recovery* experiments, the sample was subjected to a constant shear stress, $\tau$, varied between 20 and 2000 Pa for a duration of 20 s. Afterwards, the stress was removed and the recovery of the deformation in the sample was monitored for up to 3600 s (usually the recovery period was set to 100 s). For the *stress-relaxation* tests, the sample was subjected to a constant shear strain, $\gamma$, varied between 0.1% and 30%. The resulting stress and its relaxation over a given period (between 300 and 3600 s) were measured. The experimental data were analyzed using generalized Maxwell and Kelvin-Voigt rheological models, as described in detail in the following section, to determine the simplest rheological model capable of accurately describing the observed behavior and extracting the characteristic relaxation times governing the processes occurring in the samples.

Two types of oscillatory tests were also carried out to measure the

shear moduli dependence on the applied shear strain or temperature, and to compare them with those calculated from the results obtained in the relaxation tests and their description with the chosen rheological model. In the *amplitude sweep* experiments, the sample was subjected to oscillatory strain with an amplitude varying from 0.01% to 1% at a fixed frequency of 1 Hz. Oscillatory deformations upon constant temperature change were also performed. In this case, the sample was cooled from melt to the desired temperature at a constant rate, while subjected to oscillatory deformations with a fixed shear strain $\gamma = 0.02\%$ at a frequency of 1 Hz.

All parameters were chosen after performing series of preliminary tests to determine the most suitable experimental conditions. All results shown in the paper were averaged from at least three independent measurements, carried out under equivalent conditions. The error bars represent the standard deviations between the obtained experimental results. All experiments were carried out in the temperature range of rotator phase existence for the studied alkane, unless otherwise noted explicitly.

Differential scanning calorimetry measurements were performed on Discovery DSC 250 apparatus (TA Instruments, USA) to determine the phase transition temperatures. The experimental procedure was identical to that applied in our previous study [27].

## 3. Experimental results and discussion

### 3.1. Relaxation experiments in the linear viscoelastic region

The rotator phases generally exhibit viscoelastic properties. This behavior can be observed in the strain-time curves obtained in the creep-recovery experiments, see Fig. 1 for results with $C_{19}$ and Supplementary Figure S3 for results with $C_{28}$. Fig. 1**a** shows the original $\gamma(t)$ data obtained in creep-recovery experiments performed at the same temperature, in this case $T = 25°C$, but with different constant stresses, $\tau_C$, applied during the creep stage. During the creep stage (the first 20 s of the experiments), the strain does not reach a constant value instantaneously. This result suggests that the rheological response of the sample is not purely elastic. Once the applied stress is removed, the deformation decreases steeply in the first few seconds (usually between 20 and 25 s), after which the decrease becomes very slow. At longer recovery periods, usually no residue strain is observed. The quick decrease of the deformation after the removal of the stress shows the immediate elastic response of the sample, whereas the viscous properties of the material retard its complete recovery.

Results shown in Fig. 1**a** illustrate also that the maximum deformation reached during the creep stage increases with the increase of $\tau_C$, it is $\gamma_{max} \approx 0.46\%$ for $\tau_C = 500$ Pa and about 5 times lower for $\tau_C = 100$ Pa. The proportionality of the maximum strain to the applied stress shows that these stresses cause deformations which do not change the general structure of the sample, *i.e.* the experiments are performed in the linear viscoelastic region. This is even better demonstrated by the shear

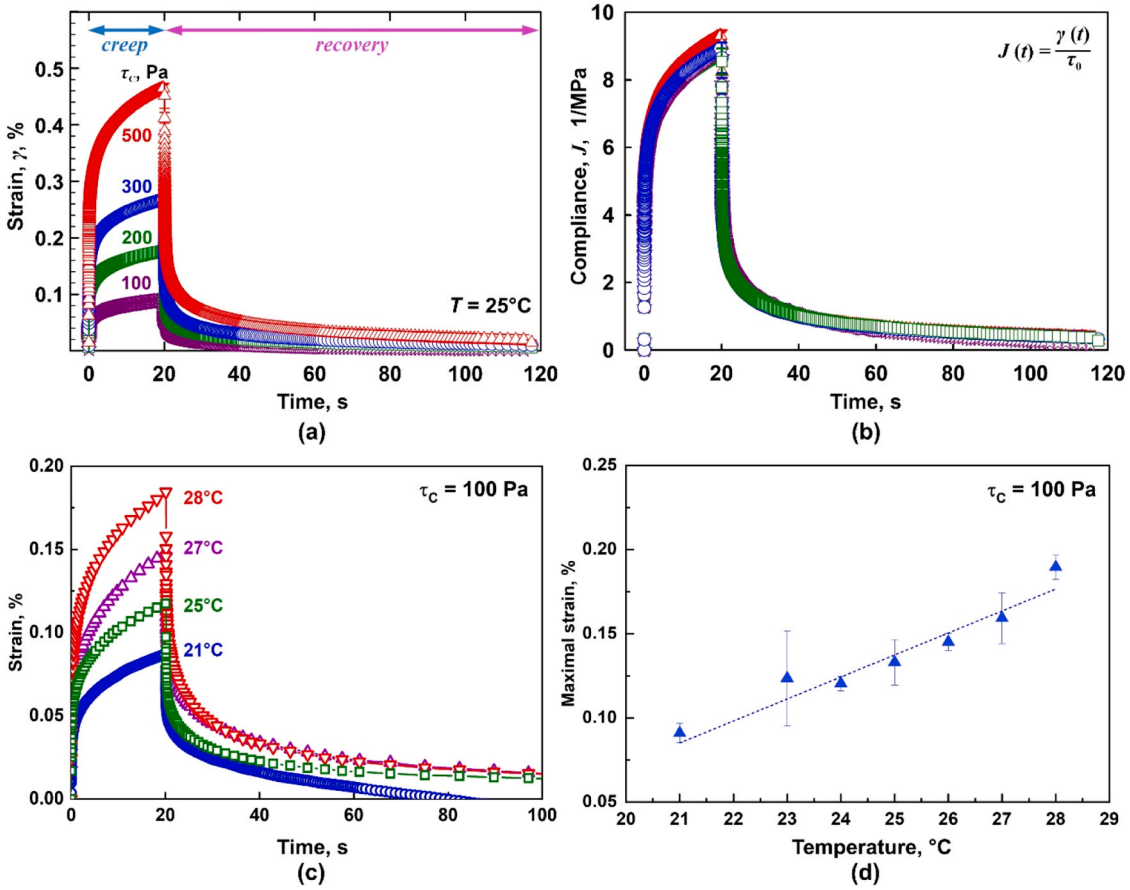


**Fig. 1.** Results obtained from creep-recovery experiments with nonadecane. (a,b) Effect of the applied stress. **(a)** Rheological curves showing $\gamma(t)$ dependence for the rotator phase of $C_{19}$, studied at 25°C at different applied stresses during the creep stage: red triangles: 500 Pa; blue circles: 300 Pa; green squares: 200 Pa; purple stars: 100 Pa. **(b)** The same experimental results as (a), presented as compliance *vs.* time. All curves fall on a master plot. **(c)** Effect of temperature for the observed strain when a fixed stress of 100 Pa is applied. The different colors represent data obtained at different temperatures: 28°C in red, 27°C in purple, 25°C in green, and 21°C in blue. **(d)** Maximum strain reached in creep-recovery experiments performed at different temperatures at a fixed applied stress of $\tau_C = 100$ Pa.

compliance function, $J(t) = \gamma(t)/\tau_C$, equal to the measured shear strain divided by the applied shear stress, see Fig. 1**b**. We note that such master curve is obtained only when the applied stresses do not cause irreversible deformation of the sample. When a critical value of the maximum strain was exceeded, the experimental results from the creep-recovery tests expressed as a compliance *vs.* time did not fall on a master curve, see Supplementary Figure S4. The critical maximum strain was found to depend slightly on the temperature, but in most cases, it was around 3–5%, see Supplementary Figure S5.

The rotator phases of the studied alkanes exist in a relatively wide temperature ranges, *e.g.* between *ca.* 21 and 32°C for $C_{19}$. Therefore, next we studied the temperature effect for the rheological properties of the rotator phases. Fig. 1**c** presents data obtained at different temperatures at a fixed value of the applied stress, $\tau_C = 100$ Pa. At higher temperatures, the sample is deformed more easily compared to lower temperatures: at 28°C, $\gamma_{max} \approx 0.19\%$, while at 21°C the maximum strain is around two times lower, $\gamma_{max} \approx 0.09\%$. As seen from Fig. 1**d**, the dependence $\gamma_{max}(T)$ is almost linear. This trend is related to the mechanical strength dependence of the temperature. At higher temperatures, the alkane molecules have higher thermal energy, they rotate more freely and make the sample easier to deform. In contrast, at low temperatures the energy of the system decreases, the number of structural defects also decreases, due to the lower concentration of non-planar conformers [28], hence smaller deformations are observed when an equivalent stress is applied. Similar results were obtained in the creep-recovery experiments, performed with the longer $C_{28}$ alkane, see Supplementary Figure S3.

Next, we studied the visco-elasto-plastic behavior of the same rotator phases by performing stress-relaxation experiments. In these tests, the sample is quickly deformed to a given shear strain value, after which the strain is held constant for a pre-defined period of time. The resulting shear stress is measured during this period. A typical example for the stress *vs.* time curve obtained in these experiments is presented in Fig. 2**a**. The maximum stress in the samples is observed when the strain approaches the pre-defined value. This happens in about 0.5–2 s after the beginning of the experiment. Afterwards, the stress begins to decrease. The steepest decrease proceeds in the initial seconds, with more than half of the maximal stress released during the first 5 s. This fast relaxation shows the visco-elastic response of the sample with the shortest relaxation time. Due to additional relaxation processes with longer relaxation times, afterwards the stress continues to decrease at a slower rate. Even after 60 min, however, the stress does not diminish to zero; instead, a relatively constant value is established, see Fig. 2**b** and Supplementary Figure S6. This result shows that the rheological model able to describe the observed behavior should contain an elastic element (spring) which is not connected to a dashpot element. This spring will account for the stress remaining in the sample upon stress-relaxation experiment after infinitely long time has passed.

The residue stress generated in the sample increases its value when the applied strain is increased for $\gamma \leq 5\%$. In contrast, the residue stress observed in the experiments was found to decrease for $\gamma > 5\%$, see Fig. 2**c** and Supplementary Figure S5. This effect is easily seen when the

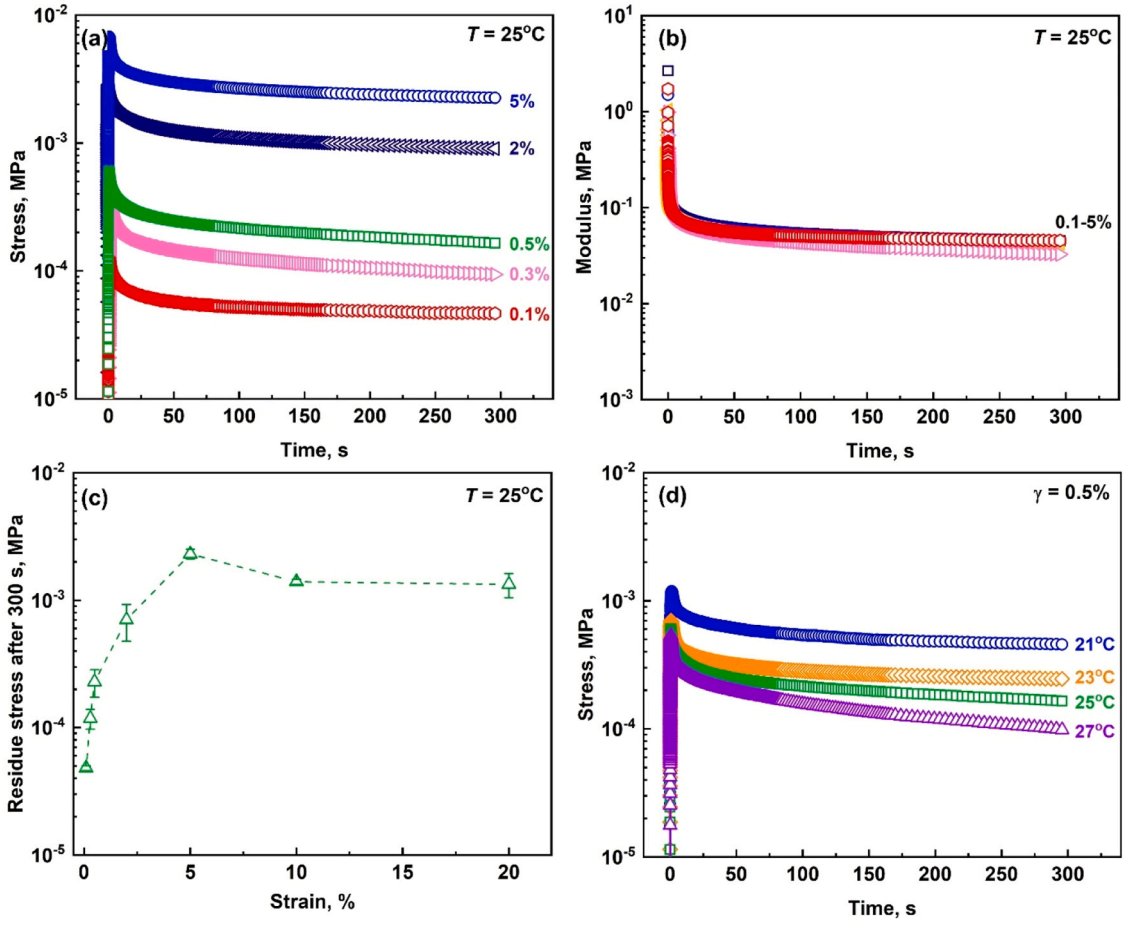


**Fig. 2.** Illustrative results obtained from stress-relaxation rheological tests with $C_{19}$ alkane. (a) Shear stress *vs.* time. (b) Modulus *vs.* time. Different colors represent the different shear strains tested, $\gamma$: 0.1% red, 0.3% pink, 0.5% green, 2% dark blue, and 5% blue. All experiments are performed at 25°C temperature. (c) Residue stress determined after 300 s relaxation time *vs.* applied shear strain. An increase is observed for $\gamma \leq 5\%$, whereas at higher shear strains it decreases due to irreversible changes proceeding in the samples. (d) Shear stress *vs.* time for experiments performed at shear strain = 0.5% at different temperatures: 21°C blue circles, 23°C orange rhombi, 25°C green squares, and 27°C purple triangles.

data are presented as the ratio between the resulting stress divided by the applied strain as a function of time. All data obtained for strains up to *ca.* 5% lie on a master curve in this scale, see Fig. 2**b**, whereas the modulus measured at higher strains have lower values, Supplementary Figure S5. This result shows unambiguously that the high strains cause changes in the overall structure of the sample, such as plastic deformations with domain restructuring, breakup of the structure, *etc.* Note that this result is identical to the differences in the compliances observed in the creep-recovery rheological tests, when stresses higher than the critical one, are applied.

Similarly, to the creep-recovery results, the stress-relaxation tests revealed a temperature dependence of both the maximum stress and the residue stress after 300 s. For experiments performed at a given shear strain, the maximum stress decreased as the temperature increased as shown in Fig. 2**d**.

In conclusion, the relaxation rheological tests performed with alkanes, structured in a rotator phase, showed that these phases exhibit elasto-visco-plastic behavior. The structure of the sample remained intact when the strain in the sample remained around or below 5%, whereas higher values resulted in plastic deformations, causing irreversible changes in the sample structure. Furthermore, the absence of residue deformation in the creep-recovery tests and the presence of residual stress in the stress-relaxation rheological experiments demonstrate that the rheological model which should be used to describe the observed behavior should contain an individual spring element.

### 3.2. Main characteristics of obtained experimental data

The experimental data from creep-recovery experiments were plotted as the logarithm of compliance, ln$J$ *vs.* the logarithm of time, ln$t$, in Supplementary Figure S7 for the entire creep region. Two distinct regions are observed in ln$J$ *vs.* ln$t$ dependence: a primary creep region, where the rate of compliance gradually decreases over time and a secondary region where a linear dependence between ln$J$ *vs* ln$t$ is established. This second region is known in the literature as secondary or Andrade creep [29–34] and it has been observed in numerous materials such as gels [35], colloidal glasses [36], microgel pastes [37], papers [38], ice crystals [39], alloys [40], rocks [41] and other materials.

The experimental data for time scales between 1 and 20 s were assumed to follow a power law dependence, *i.e.* $J = At^m$, where $A$ and $m$ are unknown constants. From the best linear fit of ln$J$ *vs.* ln$t$ the values of the constant were determined ($A$ from the intercept, and $m$ from the slope). The calculated slope values are $m = 0.18 \pm 0.04$ for $C_{19}$ samples and $0.23 \pm 0.04$ for $C_{28}$ samples, indicating that the plastic deformation is more important for rotator phases formed from the longer chain alkane. However, both of these values are lower compared to the characteristic value for Andrade creep, which is equal to 1/3, which is typically reported for samples subjected to stress levels approaching their yield stress value. The lower values determined here suggest that the applied stresses are significantly below the yield stress for the studied samples. The $m$-values determined in our study are in good agreement with values reported in the literature for shear hardening gels at shear stress below the yield stress [35]. Numerical simulations have recently predicted a continuous change for $m$ from 0 to 0.6 [34] arising from the interplay between the thermal activation and elastic stress redistribution. Values of $m$ close to 0 imply that the dislocation events are rare and the changes in the material properties are minimal during the creep period. Therefore, we conclude that the change in the material properties of studied rotator phases is limited during the creep region.

Another characteristic which can be extracted from these results is the activation energy, $E_a$, of dislocation events. To estimate this activation energy, we employed the equation proposed in Ref. [34,41]:

$$\frac{dJ}{dt} = B\exp\left(-\frac{E_a}{RT}\right)t^{m-1} \quad (1)$$

where $B$ is a material constant, $E_a$ is a material-dependent but stress independent activation energy, $R$ is the universal gas constant and $T$ is the temperature. The dependences of ln($Am$) *vs.* ln(1/$T$) for $C_{19}$ and $C_{28}$ phases are shown in Fig. 3. From the slope of the curves, we determined $E_a \approx 70 \pm 20$ kJ/mol for $C_{19}$ and $E_a \approx 170 \pm 40$ kJ/mol for $C_{28}$. These values represent the activation energies for self-diffusion [41].

Self-diffusion in closely packed alkanes is assumed to proceed by self-diffusion of vacancy rather than interstitial migration [42,43]. It is known that the activation energy for self-diffusion is in the order of heat of sublimation [42,43]. The heat of sublimation of $C_{19}$ alkane is 140 kJ/mol and 240 kJ/mol for C28 alkane [44]. The experimentally determined values for the self-diffusion activation energy are around twice smaller as compared to the heat of sublimation. This discrepancy most probably occurs because the activation energy for vacancy self-diffusion in rotator phases is lower than in the well-ordered crystalline phases. Note that the sublimation energy for $C_{20}$ alkane is 170 kJ/mol, whereas the activation energy for self-diffusion in rotator phase is measured to be 83 kJ/mol [45] which is again twice smaller. Therefore, we can conclude that the linear stage in creep experiments is related to the self-diffusion of the vacancies which have the activation energy around twice smaller as compared to their activation energy in the well packed crystals.

The next stage was to examine the sample behavior during the recovery phase. Recovery compliance is defined as $J_{rec}(t) = (\gamma(t_{CR}) - \gamma(t + t_{CR}))/\tau_C$ [46], where $\gamma(t_{CR})$ is the maximum strain reached during the creep stage and $\gamma(t + t_{CR})$ is the strain measured during the recovery. To facilitate comparison, the recovery time was redefined to start from zero. The data from Fig. 1**b** is replotted in Supplementary Figure S8 on a logarithmic scale for both parts (creep and recovery). The creep and recovery data fall on the same master curves for experiments performed between 100 and 500 Pa demonstrating that the transient deformations are recovered upon removal of the stress. At longer time scale, ln$J_{rec}$ levels off as the strain fully recovers.

The data for ln$J_{rec}$ *vs.* ln$t$ between 1 and 20 s after removing the stress were used to determine the values of $A_{rec}$ and $m_{rec}$, which characterize the expression $J_{rec} = A_{rec}t^{mrec}$. The values for $m_{rec}$ were determined to be slightly lower than those determined from the creep part: $m_{rec} \approx 0.15 \pm 0.03$ for $C_{19}$ and $0.20 \pm 0.04$ for $C_{28}$, while the activation energies during the relaxation part were found to be consistent with those from the creep phase. This confirms that the processes driving strain increase during the creep are reversible upon stress removal and possess similar activation energies.

The stress-relaxation experiments demonstrate that the tested materials behave as viscoelastic solids, as seen by the presence of residual stress under constant strain deformation. When the experimental data from Fig. 2**a** are replotted on a logarithmic scale in Supplementary Figure S5c, it becomes evident that the residual stress is a linear function of the applied strain up to ca. 5% strains. Based on the slope of the curve, the residual modulus is determined to be $43 \pm 5$ kPa for strains up to 5%. This value implies the presence of a spring that is not attached to a dashpot, preventing the complete relaxation during the stress-relaxation experiments and ensuring recovery during the creep-recovery rheological tests. Finally, the observed decrease in the residual stress values as deformation increases toward 10% (see Supplementary Figure S5b,**c**) indicates that the material begins to yield at these higher strain levels which leads to a significant decrease in both the residual stress and residual modulus. This observation suggests that the elastic nature of the rotator phases begins to transform once the strain exceeds ca. 5%, a phenomenon likely related to an irreversible sliding of rotator phase domains under higher deformations.

Next, we describe how a model containing the smallest number of parameters was chosen and applied to describe the observed rheological behavior in the linear viscoelastic regime ($\gamma < 5\%$).

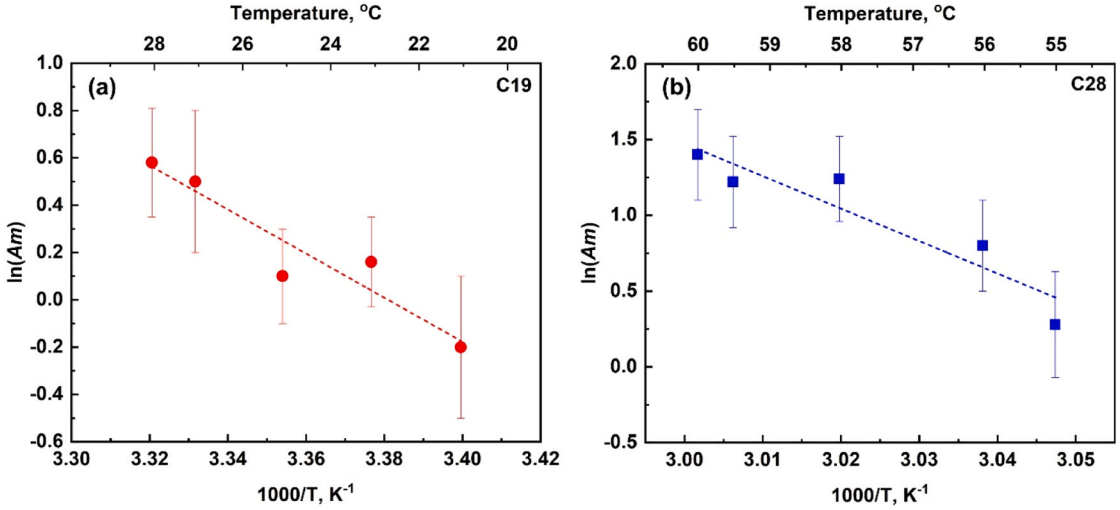


**Fig. 3.** Ln (*Am*) *vs.* 1000/T for: (a) $C_{19}$, and (b) $C_{28}$ samples.

### 3.3. Selection of an appropriate rheological model for data description

The rheological properties of the viscoelastic materials are usually described by compositional rheological models composed of elastic (springs) and viscous (dashpots) elements connected in various ways. The simplest mathematical models used to describe the viscoelastic properties of materials are the Maxwell and Kelvin-Voigt models [47–49]. These models describe the behavior of materials showing one characteristic relaxation time only. For the rotator phases, however, a model having at least two characteristic times is needed to describe the initial quick and the later much slower relaxations, observed in the stress-relaxation and creep-recovery rheological experiments, see Figs. 1 and 2. Therefore, the applicability of a generalized viscoelastic model, connecting several Kelvin-Voigt or Maxwell elements, was investigated for description of the experimental results.

Note that every generalized Kelvin-Voigt (GKV) model has an equivalent generalized Maxwell (GM) model – these two models are linked by the Prony series adjusting the creep and relaxation functions [50]. To interpret the experimental results from creep-recovery and stress-relaxation tests, we employed the Generalized Maxwell (GM) and Generalized Kelvin-Voigt (GKV) models. Although these two models are mathematically equivalent, we selected specific model for given experimental data sets to simplify the analytical description. We analyzed the stress-relaxation data using analytical expressions derived from the GM model, which is also commonly referred to as the Maxwell-Wiechert model [47,50]. Once the elasticities of the springs and the viscosity of the dashpots were determined for the GM model, these parameters were converted into their GKV equivalents to ensure a consistent representation of the stress-relaxation behavior. On the other hand, we analyzed the creep-recovery data by first determining the GKV parameters through its corresponding analytical expressions and then calculating the equivalent GM parameters. This approach allowed us to obtain a complete set of parameters for both models for both stress-relaxation and creep recovery experiments, ensuring that the viscoelastic characteristics of the studied rotator phases were fully captured regardless of the specific test performed.

Finally, on the basis of physicochemical arguments, we discuss which of the two (mathematically equivalent) models, GKV or GM, is more relevant for description of the specific system under investigation and provide plausible molecular interpretation of the underlying relaxation processes.

#### 3.3.1. Stress-relaxation data description under the assumption that $\gamma = const$

The simplest GM model which could potentially be used to describe our data consists of a single elastic element, connected in parallel to a single Maxwell element, a set of one dashpot and one spring, connected in a series, see GM1 part of the inset in Fig. 4**a**. The elastic moduli and viscosity characterizing each element in the model are denoted as $E_\infty$, $E_1$ and $\eta_1$. This model is also known as the Zener model and is described by the following differential equation, connecting the stress, $\tau(t)$, and strain, $\gamma(t)$, functions and their time derivatives [50]:

$$\tau + \frac{\eta_1}{E_1}\frac{d\tau}{dt} = E_\infty \gamma + \frac{\eta_1}{E_1}(E_\infty + E_1)\frac{d\gamma}{dt} \tag{2}$$

By solving this equation for the stress-relaxation experiments, a relation between the relaxation modulus, shear stress divided by the constant shear strain, $Y = \tau/\gamma_c$, the model constants, and time can be obtained for the GM1 model [50]:

$$Y = Y_0\left(1 - p_1\left(1 - e^{-\frac{t}{\lambda_1}}\right)\right) = E_\infty + E_1 e^{-\frac{t}{\lambda_1}} \tag{3}$$

$$p_1 = \frac{E_1}{E_\infty + E_1}, \tag{4}$$

where $Y_0$ is the sum of the springs constants, $Y_0 = E_\infty + E_1$, $t$ is the time, and $\lambda_1 = \eta_1/E_1$ is the characteristic relaxation time for the Maxwell element in the GM1 model. Note that this solution is obtained under the assumption that the applied shear strain is constant during the entire experiment, $\gamma = \gamma_C$ and $d\gamma/dt = 0$. Although this assumption is generally correct throughout the main part of the stress-relaxation experiment, it does not account for the real strain dependence in the first initial seconds when the strain increases from 0 up to the pre-defined constant value. An example for the actual strain dependence on time is shown in Fig. 4**b**. As seen from this graph, it takes about 3 s to obtain 99.5% of the final $\gamma_C$ value, whereas the final constant strain is obtained in about 6 s after the beginning of the experiment. This complication will be further discussed below.

The fit of the experimental data obtained after the initial few seconds of the experiments with Eq. 3 is shown with orange line in Fig. 4**a**. As seen from this comparison, GM1 model is unable to describe the experimental results, demonstrating that a more complex model is needed. Therefore, next we introduced a second Maxwell element to the model, see GM2 schematics in the inset of Fig. 4. For this model, a second exponential term is added to Eq. 3 [50]. This modification

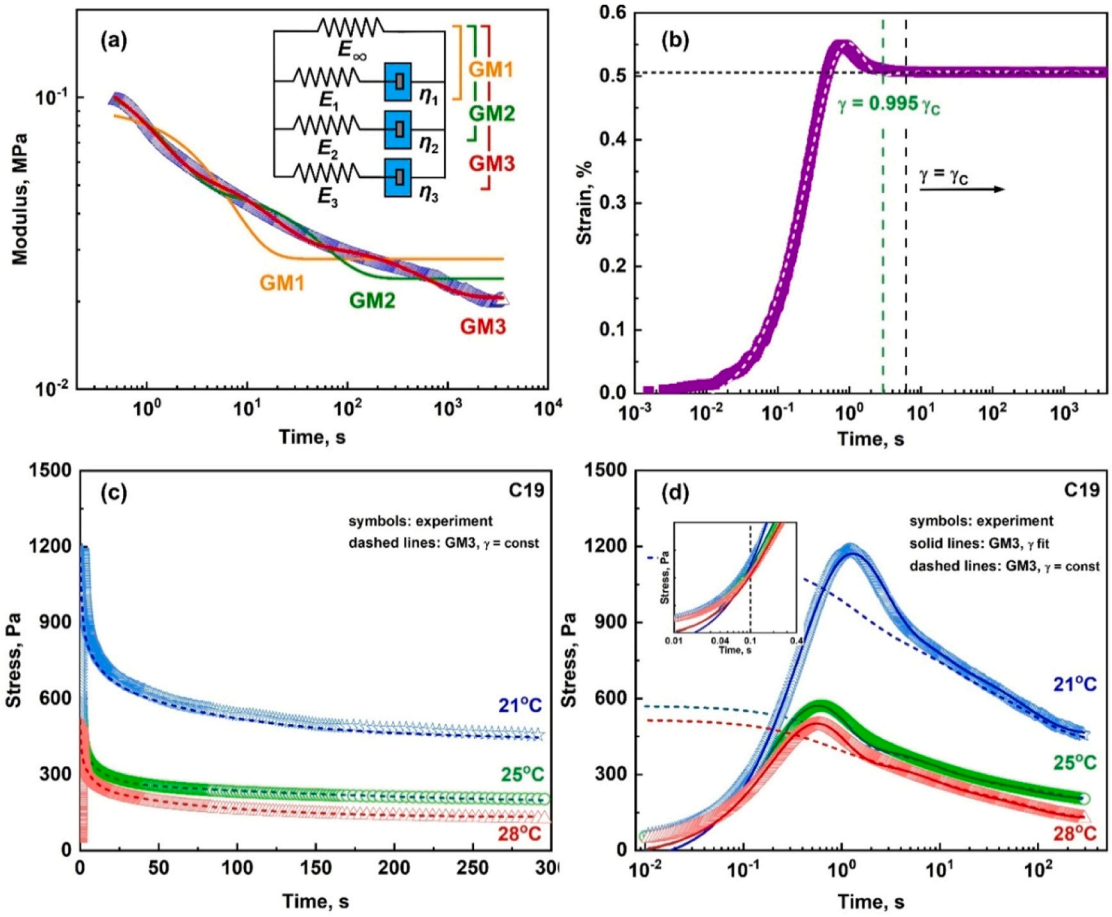


**Fig. 4.** (a) Fitting of the relaxation modulus measured in a stress-relaxation experiment with generalized Maxwell models of different orders: orange – GM1; green – GM2; red – GM3. Inset: schematic representation of the models. (b) Strain *vs.* time dependence. The experimental data shown are obtained with $C_{19}$ alkane at 27°C. The set strain value is 0.5% and the actual strain value obtained is ≈ 0.506%. The dashed white line shows the γ(t) fit, see Eq. 15 and related discussion in Section 3.3.2 below. (c,d) Stress *vs.* time dependence for nonadecane obtained in stress-relaxation experiments performed with $\gamma = 0.5\%$ at different temperatures: 21°C blue, 25°C green, 28°C red. The symbols show the experimental data; dashed lines – GM3 fit assuming that applied strain is constant throughout the whole experiment; solid lines – GM3 fit using the actual $\gamma(t)$ dependence found in the experiment. Inset in (d): zoom-in of the 0.01–0.4 s, showing the slight discrepancy between the obtained fits and the actual stress.

improved slightly the data fit, as seen by the green line in Fig. 4. However, the GM2 model was also unable to accurately describe both the rapid initial relaxation and the subsequent very slow relaxation at longer times. Moreover, the relaxation modulus predicted by the GM2 model at infinite time exceeded the experimentally observed value, indicating that two relaxation times are insufficient to fully describe the rheological behavior of the rotator phases.

Next, a third Maxwell element was added to the model, see GM3 in Fig. 4**a**. The differential equation describing the relation between the shear stress, τ, and shear strain, γ, for this model is [50]:

$$\tau + \frac{B}{A}\frac{d\tau}{dt} + \frac{C}{A}\frac{d^2\tau}{dt^2} + \frac{Z}{A}\frac{d^3\tau}{dt^3} = \frac{a}{A}\gamma + \frac{b}{A}\frac{d\gamma}{dt} + \frac{c}{A}\frac{d^2\gamma}{dt^2} + \frac{z}{A}\frac{d^3\gamma}{dt^3} \tag{5}$$

where the values of the $A$, $B$, $C$, $Z$, $a$, $b$, $c$, and $z$ constants are related to the spring and dashpot constants, $E_i$ and $\eta_i$ [50]:

$$A = E_1E_2E_3; \quad a = E_\infty A$$
$$B = E_1E_2E_3\left(\frac{\eta_1}{E_1} + \frac{\eta_2}{E_2} + \frac{\eta_3}{E_3}\right); \quad b = E_\infty B + A(\eta_1 + \eta_2 + \eta_3)$$
$$C = E_1E_2E_3\left(\frac{\eta_1\eta_2}{E_1E_2} + \frac{\eta_1\eta_3}{E_1E_3} + \frac{\eta_2\eta_3}{E_2E_3}\right); \quad c = E_\infty C + A\left(\frac{\eta_1\eta_2}{E_2} + \frac{\eta_1\eta_3}{E_3} + \frac{\eta_2\eta_3}{E_3}\right)$$
$$Z = \eta_1\eta_2\eta_3; \quad z = (E_\infty + E_1 + E_2 + E_3)Z \tag{6-9}$$

According to this model, under the assumption for a constant shear strain, the relaxation modulus is defined as [50]:

$$Y = Y_0\left(1 - \sum_{i=1}^{3} p_i\left(1 - e^{-\frac{t}{\lambda_i}}\right)\right) \tag{10}$$

where $Y_0$ represents the sum of the elastic constants:

$$Y_0 = E_\infty + E_1 + E_2 + E_3 \tag{11}$$

The constants $p_i$ are defined as:

$$p_i = \frac{E_i}{Y_0} \tag{12}$$

and $\lambda_i = \eta_i/E_i$, $i = 1$, 2 or 3 are the characteristic times for the individual Maxwell elements in the GM3 model.

Using the GM3 model, we were able to describe sufficiently well the main trends in the experimentally obtained relaxation curve, see the red line in Fig. 4**a**. To evaluate the applicability of the GM2 and GM3 models in fitting the experimental data, we calculated the Akaike Information Criterion (AIC) and Bayesian Information Criterion (BIC) values [51]. The AIC and BIC values determined for the GM2 model were consistently higher by a magnitude of 1000 compared to those for the GM3 model, indicating an approximately 100% probability that GM3 is the superior model. Furthermore, we analyzed the p-values of the estimated

parameters. When using the GKV3 and GM3 models, *p*-values were typically within the range of $10^{-50}$, suggesting that all included parameters are statistically significant and essential for describing the experimental data. Only at high stress levels and elevated temperatures did the *p*-values for the third element increase to approximately $10^{-2}$ for certain samples. We also attempted to fit the data using GKV4 and GM4 models. However, the p-values for the newly added parameters exceeded 0.1, indicating that these additional variables could not be determined with a sufficient accuracy or reliability. Consequently, this statistical analysis confirms that the GKV3 and GM3 models represent the most appropriate choice for interpreting our experimental results.

Similar analyses using GM3 model were performed for the stress-relaxation data obtained in more than 120 independently performed experiments with nonadecane and octacosane samples at different temperatures, falling within the temperature range of rotator phase existence. Data from experiments, for which the modulus fall on a master curve under the studied temperature, were used only. From the performed analyses, we were able to calculate the elastic and viscous constants of the springs and dashpot elements, $E_i$ and $\eta_i$, and the three characteristic relaxation times. These parameters were further used to calculate the storage, $G'$, and loss, $G''$, moduli for the rotator phases using the following relations [50]:

$$G' = Y_0\left[1 - \sum_{i=1}^{3}\left(\frac{p_i}{1+\lambda_i^2\omega^2}\right)\right]$$
$$G'' = \sum_{i=1}^{3}\frac{\eta_i\omega}{1+\lambda_i^2\omega^2} \quad (13\text{-}14)$$

where $\omega$ is the angular velocity.

Fig. 4**c,d** and Supplementary Figure S9a show illustrative comparison between the experimental results and their theoretical fit using GM3 model (see the dashed lines). These fits were obtained using the experimental data collected after the first few initial seconds, once the desired strain value had become established. As seen from Fig. 4**c** and Supplementary Figure S9a, the data description after the first few seconds is excellent. However, a closer look into the first few seconds of the experiment reveal a noticeable deviation between the system response predicted by the current model and that observed experimentally, see Fig. 4**d**.

This discrepancy arises due to the inaccurate assumption, used to derive the equations used for this theoretical description. As already explained, Eq. 10 describes the moduli under the assumption that the applied shear strain is constant during the entire experiment. Although this assumption is valid about 3–6 s after the beginning of the experiment, see Fig. 4**b** and Supplementary Figure S9b, it is inaccurate during these initial seconds. This inconsistency makes the extrapolated data description also inaccurate during these first several seconds, which results in artificially lower value of the elastic constant $E_1$ and in higher values of the characteristic time $\lambda_1$. To correct this deviation, next we developed a model accounting for the experimentally measured time dependence of the strain applied to the sample.

### 3.3.2. *Stress-relaxation data description using the experimentally measured $\gamma(t)$ dependence*

Instead of being constant during the entire stress-relaxation experiment, the strain function needs several seconds to increase and then to establish the constant value, set in the experimental protocol, see Fig. 4**b**. Note that $\gamma(t)$ function shows a small overshooting above the experimentally set value, after which it returns to the desired value. Our analysis of the rheological data showed that such behavior is observed in practically all stress-relaxation experiments. Therefore, to correctly estimate the characteristic constants related to the first Maxwell element present in the GM3 model (which will react the fastest), we need to describe correctly the complete strain-time dependence.

With this aim, we first described $\gamma(t)$ dependence for a given experiment, using the following analytical function:

$$\gamma(t) = k_1\left(1 - e^{-k_2 t}\right) - (k_3 t + k_4)e^{-k_5 t} \quad (15)$$

where $k_i$ are numerical constants. Examples showing the obtained $\gamma(t)$ fits are shown with curves in Fig. 4**b** and Supplementary Figure S9b. Afterwards, a Laplace transform from the time domain to the Laplace domain was performed for $\gamma(t)$ and $Y(t)$ functions, and the differential equation relating the strain and stress functions was solved numerically using two unknown variables, $E_1$ and $\lambda_1$. The other constants from the GM3 model were held constant with the initial estimate made by the experimental data description in the time domain (namely, the fit shown in Fig. 4**a,c**). Once $E_1$ and $\lambda_1$ constants were calculated, an inverse Laplace transform was applied to $\gamma(s)$ and $Y(s)$ functions to return them to the real-time domain. Afterwards, a second fitting procedure was applied to the experimental data, obtained after the constant strain value had been already established in the system. For this fit, the initial simpler version of the $Y(t)$ function was used, see Eq. 10.

A comparison between the data fit obtained under the assumption for $\gamma(t) = \text{const}$ (dashed lines) and the one obtained with the actual $\gamma(t)$ dependence (solid lines) is presented in Fig. 4**d**. As seen from these fits, the deviation in the description of the experimental results with the constant strain value, seen in the initial few seconds, has been (almost) resolved when the real $\gamma(t)$ function is used, providing us with an accurate description of the entire $Y(t)$ dependence, as well as with correct $E_i$ and $\eta_i$ values, and $G'$ and $G''$ moduli. A small deviation during the initial ca. 0.1 s still remains, see the inset in Fig. 4**d**. However, it probably arises from the imprecision of the rheometer response at very short times, as the chosen model is able to describe the creep-recovery data very well.

Detailed analysis of the obtained parameters, their temperature and alkane chain length dependences are presented in **Section 3.5**. Before that, we explain how the creep-recovery results were analyzed with the GM3 and GKV3 models to compare the parameters obtained from the data fitting by the two types of rheological tests, described in Section 3.1 (Figs. 1 and 2).

### 3.3.3. *Creep-recovery data description with GM3 and GKV3 models*

Considering that the simpler GM1 and GM2 models were unable to describe sufficiently well the experimental results from the stress-relaxation tests, and that the chosen rheological model should be able to describe both the creep-recovery and stress-relaxation results, we will not present the analysis of the GM1 and GM2 models of the creep-recovery tests. Instead we explain directly the applicability of the GM3 model.

As already explained, the generalized Maxwell and Kelvin-Voigt models comprising the same number of elements (springs and dashpots) are equivalent [50]. As the data description for the creep-recovery experiments is more straightforward using the GKV model, we first used this model to describe the obtained experimental results.

A schematic picture of the GKV3 model is shown as inset in Fig. 5. Note that although the elements included in the GM3 and GKV3 models are identical, the different way in which they are connected to one another makes their elastic and viscous constants different. To easily distinguish the rheological parameters in the GM3 and GKV3 models, we use the $E_i$, $\eta_j$ and $\lambda_j$ notation for the GM3 parameters, whereas to describe the GKV3 model we denoted the springs constants with $G_i$, the dashpot constants with $\mu_j$, and the characteristic relaxation times with $t_j = \mu_j/G_j$, where $i = 0$–3 and $j = 1$, 2 or 3.

The differential equation describing the stress-strain relation for the GKV3 model is [50]:

$$\tau + \frac{B_1}{A_1}\frac{d\tau}{dt} + \frac{C_1}{A_1}\frac{d^2\tau}{dt^2} + \frac{Z_1}{A_1}\frac{d^3\tau}{dt^3} = \frac{a_1}{A_1}\gamma + \frac{b_1}{A_1}\frac{d\gamma}{dt} + \frac{c_1}{A_1}\frac{d^2\gamma}{dt^2} + \frac{z_1}{A_1}\frac{d^3\gamma}{dt^3} \quad (16)$$

Note that Eq. 16 is identical to Eq. 5 describing the GM3 model. The constants multiplying the stress and strain derivatives, however, have

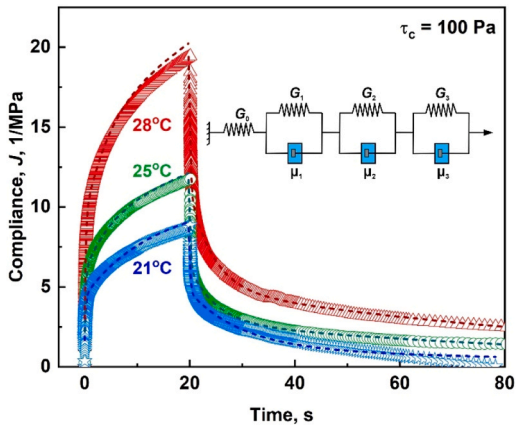


**Fig. 5.** Illustrative graphs showing the experimental data fitting with GKV3 model. Experimental data are shown with empty symbols, whereas the fits are plotted with dashed lines. Results from creep-recovery experiments performed with $C_{19}$ alkane at $\tau_c = 100$ Pa are shown. Inset: Schematic representation of the Generalized Kelvin-Voigt model with 3 consecutively connected Kelvin-Voigt elements, GKV3.

different values, thus the "1" subscripts were introduced in the constants in Eq. 16. Their values are [50]:

$$a_1 = G_0 G_1 G_2 G_3;$$
$$A_1 = a_1\left(\frac{1}{G_0}+\frac{1}{G_1}+\frac{1}{G_2}+\frac{1}{G_3}\right);$$
$$b_1 = a_1(t_1+t_2+t_3);$$
$$B_1 = \frac{b_1}{G_0} + a_1\left(t_1\left(\frac{1}{G_2}+\frac{1}{G_3}\right)+t_2\left(\frac{1}{G_1}+\frac{1}{G_3}\right)+t_3\left(\frac{1}{G_1}+\frac{1}{G_2}\right)\right) \quad (17\text{-}20)$$
$$c_1 = a_1(t_1t_2+t_1t_3+t_2t_3);$$
$$C_1 = (G_0+G_1)\mu_2\mu_3+(G_0+G_2)\mu_1\mu_3+(G_0+G_3)\mu_1\mu_2$$
$$z_1 = G_0\mu_1\mu_2\mu_3; \quad Z_1 = \mu_1\mu_2\mu_3$$

The creep compliance in the GKV3 model can be expressed as [52]:

$$J_{cr}(t) = \frac{1}{G_0}+\frac{1}{G_1}\left(1-e^{-\frac{t}{t_1}}\right)+\frac{1}{G_2}\left(1-e^{-\frac{t}{t_2}}\right)+\frac{1}{G_3}\left(1-e^{-\frac{t}{t_3}}\right) \quad (21)$$

and the recoverable compliance is [53]:

$$J_r(t) = \left(1-e^{-\frac{t_{cr}}{t_1}}\right)e^{-\frac{t-t_{cr}}{t_1}}\frac{1}{G_1}+\left(1-e^{-\frac{t_{cr}}{t_2}}\right)e^{-\frac{t-t_{cr}}{t_2}}\frac{1}{G_2}+\left(1-e^{-\frac{t_{cr}}{t_3}}\right)e^{-\frac{t-t_{cr}}{t_3}}\frac{1}{G_3} \quad (22)$$

where $t_{cr}$ denotes the creep period set in the experiment.

Using Eqs. 21 and 22, the creep-recovery data were analyzed and $G_i$, $\mu_j$ and $t_j$ constants were calculated. An example for the fit obtained using these equations is presented in Fig. 5. The calculation of the storage and loss moduli for the GKV3 model, however, is not straightforward as in the case of GM3 model. Therefore, to compare the parameters of creep-recovery and stress-relaxation tests, we developed a procedure allowing us to calculate the $E_i$, $\eta_i$ and $\lambda_i$ constants using the $G_i$, $\mu_j$ and $t_j$ values and vice versa. The calculation of the GKV3 model constants ($G_i$, $\mu_j$, $t_j$) from the experimental results described with the GM3 model (i.e. stress-relaxation experiments) is described in details in Supplementary Information **Section A**.

For the calculation of the GM3 constants ($E_i$, $\eta_i$, $\lambda_i$) from the GKV3 constants we used the same procedure but in a reverse order. The $E_i$, $\eta_i$ and $\lambda_i$ constants determined from the GM3 model fits of the experimental data were used along with equations 13–14, to determine the storage and loss moduli for the system. The obtained values are presented and discussed in the next sections.

### 3.4. Storage and loss moduli for rotator phases of alkanes

The storage and loss moduli for a given visco-elastic material indicate its ability to store energy elastically and to dissipate energy, respectively. They present a combined characteristic of the different elastic and viscous contributions which may be described using a more detailed rheological model. To further demonstrate the applicability of the used GM3 and GKV3 models, we compare the storage and loss moduli calculated using the third-order models description of the stress-relaxation and creep-recovery data for the rotator phases of alkanes, with the values measured in independent oscillatory rheological tests, see Fig. 6.

An excellent agreement between the storage and loss moduli calculated from the creep-recovery (CR) and stress-relaxation (SR) results analysis with the third-order generalized Kelvin-Voigt and Maxwell models is observed with the $G'$ and $G''$ moduli measured directly in oscillatory type of experiments, Fig. 6. Furthermore, as previously shown in Ref. [27], the storage modulus is higher than the loss modulus for the rotator phases of both alkanes and the values of these moduli increase with the temperature decrease.

The importance of the precise data description and the usage of complete $\gamma(t)$ dependence in the analysis of the stress-relaxation tests is demonstrated in Fig. 6. The orange crossed triangles show the moduli calculated from the stress-relaxation data description, under the assumption that the applied strain is constant throughout the whole experiment (i.e. disregarding the data from the initial few seconds in which the constant strain has not been established yet). In contrast, the red triangles show the corrected moduli determined using the complete $\gamma(t)$ dependence. While the red triangles coincide well with the data from the other types of experiments, a significant discrepancy is observed for the data obtained under the constant strain assumption. The observed deviation is especially significant for the values of the loss moduli which become about 3–10 times higher when the complete $\gamma(t)$ dependence is accounted for.

This comparison confirms that the third-order models are applicable for description of the visco-elastic behavior of rotator phases of alkanes. Therefore, next we analyze the parameters values calculated from the description of the SR and CR results with the GM3 and GKV3 models.

### 3.5. GM3 vs. GKV3 model – relevance to the presently investigated system. Comparison of the viscous and elastic parameters

Each of the third-order generalized Kelvin-Voigt (GKV3) and Maxwell (GM3) rheological models contains seven elements – three spring-dashpot pairs, and an additional spring. Although the constituent elements are identical and the models have been proven to be mathematically equivalent [50], the models are derived from fundamentally different physical assumptions. GM3 would describe correctly the shear with the same local deformation everywhere, whereas GKV3 would describe correctly a shear with the same local stress everywhere. In reality, in a complex domain structure with softer interdomain regions both the deformation and the stress could vary locally. Therefore, the constants obtained from experimental data description with both models are described in the paper. However, we argue that due to the softer regions of disordered molecules and disordered terminal molecular fragments, one could not expect the local deformation to be the same everywhere in the rotator phase samples studied here. Thus, we give some preference to GKV3 model, while admitting that the stress and strain distributions in the real sample could be more complex. As seen from the comparison of the model parameters, determined from both GM3 and GKV3 models, the numerical values of the parameters for the respective elements are close to one another – an indication that these values are robust and can be used to discuss the possible molecular relaxation mechanisms.

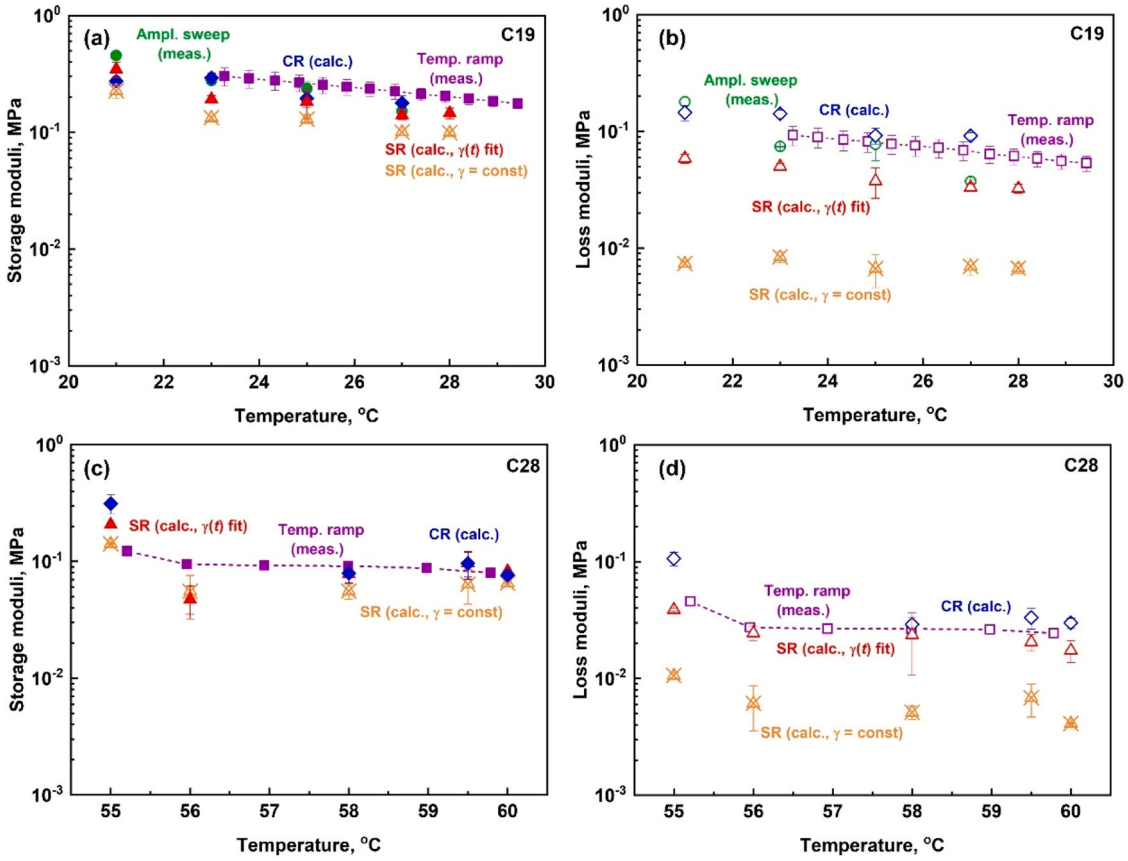


**Fig. 6.** Storage (a,c) and loss (b,d) moduli for rotator phases of $C_{19}$ (a,b) and $C_{28}$ (c,d) alkanes. Different symbols denote the data obtained in different experiments: purple squares: temperature ramps, 2 °C/min ($C_{19}$), and 1 °C/min ($C_{28}$), 1 Hz oscillation frequency; green circles: amplitude sweep experiments performed at the given temperature, data for: 1 Hz frequency, 0.02% amplitude; blue diamonds: data calculated from the creep-recovery experiments using GKV3 and GM3 models; triangles: data calculated from the stress-relaxation experiments using GM3 model under the assumption that the applied strain is constant during the entire experiment (orange crossed symbols) or using the real $\gamma(t)$ dependence, as observed experimentally (red symbols).

In GKV model, the micro-heterogeneous structure is allowed to undergo different deformations in the various micro- and nano-regions, as would be expected for such material. The assumption for uniform deformation everywhere, characterizing the GM model, would be more appropriate for homogeneous systems which is not our case. Accordingly, we present and discuss below the averaged parameters obtained from both creep-recovery and stress-relaxation experiments using the GKV3 model. For completeness, the parameters derived from the GM3 models are presented in Supplementary Figure S10. We note that all major trends identified from the GKV3 model are also observed in the GM3 analysis, although the absolute values of the elastic and viscous constants are slightly lower when the GM3 model is applied.

Fig. 7 presents the temperature dependence of the constants derived from the GKV3 model, averaged over both creep-recovery and stress-relaxation experiments. The averaged elastic and viscous constants for nonadecane (Fig. 7**a** and **c**) exhibit a pronounced temperature dependence, with their values increasing as the temperature decreased. The averaged rates of change determined between 21 and 28°C were: $dG_i/dT \approx -0.049 \pm 0.007$ MPa.°$C^{-1}$ and $d\mu_i/dT \approx -0.050 \pm 0.009$ MPa.s.°$C^{-1}$. In contrast, the larger fitting uncertainties obtained for octacosane prevented reliable determination of analogous slopes. Instead, its elastic moduli and viscous constants were found to be almost temperature-independent within the investigated range between 56 and 60°C, see Fig. 7**b,d**. This behavior is probably caused by the significantly higher fraction of non-planar (*gauche*) conformers in octacosane, compared to the shorter nonadecane, combined with the narrower temperature interval over which its rotator phase exists.

Furthermore, analysis of the elastic constants in GKV3 model showed that $G_0 \gtrsim G_1 \approx G_2 >> G_3$, see Table 1 and Fig. 7**a,b**. For nonadecane, $G_0$ was approximately 30 ± 9% higher than $G_1$ and $G_2$, which exhibited similar values at a given temperature, e.g. $G_1$, $G_2 \approx 0.19 \pm 0.05$ MPa at 28°C and 0.29 ± 0.08 MPa at 23°C. In the case of octacosane, this difference was less pronounced, and $G_0$, $G_1$ and $G_2$ constants were nearly identical within the experimental uncertainty with $G_0$, $G_1$, $G_2 \approx 0.10 \pm 0.02$ MPa in the 56–60°C temperature range. In contrast, the elastic constant associated with the fourth spring in the GKV3 model was significantly smaller: for nonadecane, $G_3 \approx 0.07$ MPa at 28°C, increasing to $\approx 0.08$ MPa at 23°C, whereas for octacosane $G_3 \approx 0.013$ MPa. These results show that the processes associated with the first two characteristic times, $t_1$ and $t_2$ have comparable elastic contributions, whereas the third process, which is the slowest one, has substantially smaller elastic contribution.

The three viscous constants, which characterize the resistance of the dashpot elements in the model, exhibited clearly distinct values. For nonadecane, $\mu_1 \approx 0.07$–$0.21$ MPa.s, $\mu_2 \approx 1.48$–$3.37$ MPa.s and $\mu_3 \approx 8.6$–$22.4$ MPa.s in GKV3 model depending on the temperature. For octacosane, these values decreased to: $\mu_1 \approx 0.04 \pm 0.01$ MPa.s, $\mu_2 \approx 0.8 \pm 0.2$ MPa.s and $\mu_3 \approx 2.4 \pm 0.6$ MPa.s, but the hierarchy $\mu_1 < \mu_2 < \mu_3$ was preserved.

Next, we discuss the relaxation times, defined as the ratios of the viscous to elastic constants, determined from the GKV3 model, and their possible relation to the molecular processes within the system.

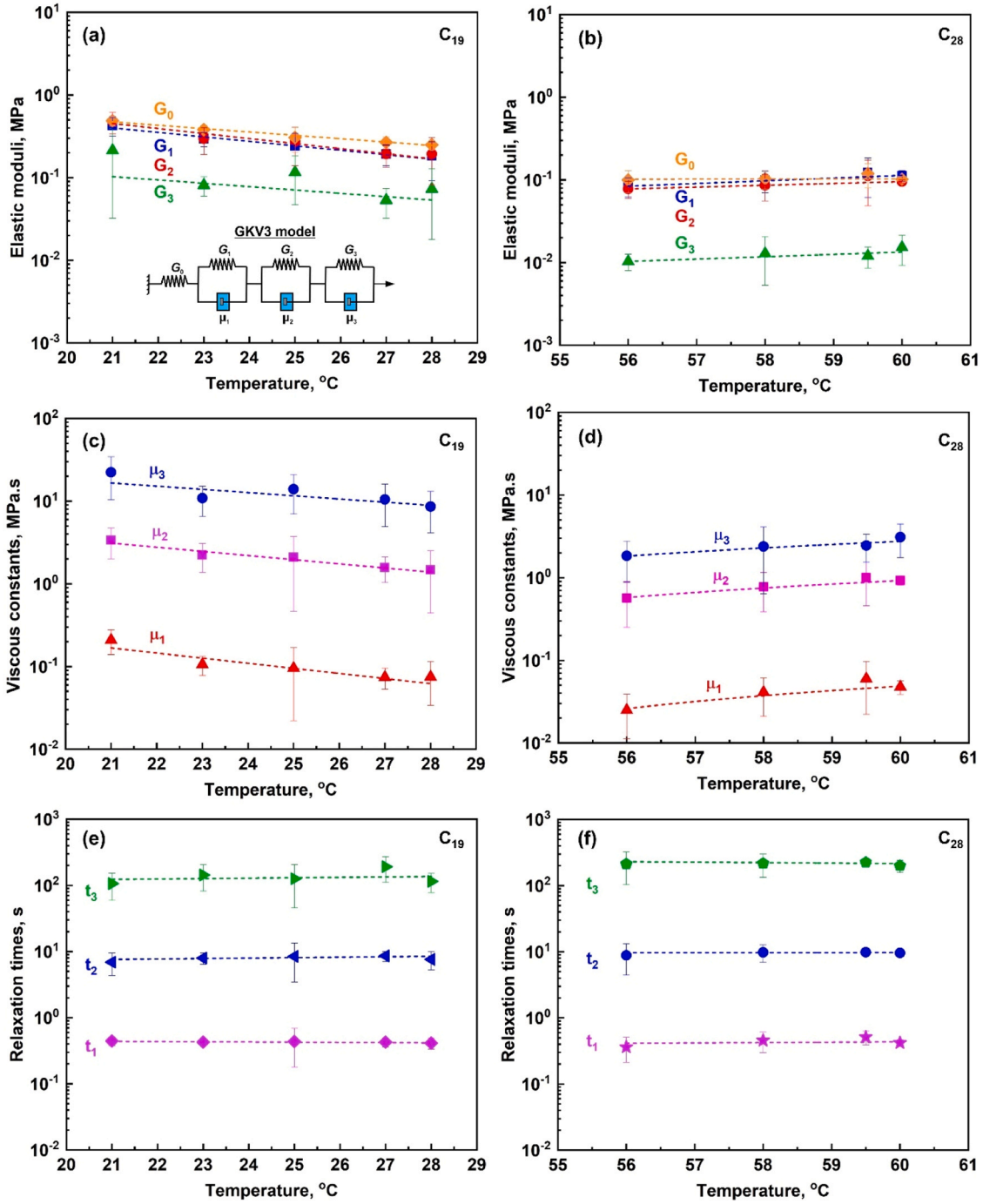


**Fig. 7.** Temperature dependence of the averaged parameters derived from GKV3 model in creep-recovery and stress-relaxation experiments. (a,c,e) $C_{19}$ alkane; (b,d, f) $C_{28}$ alkane. (a,b) Elastic constants; (c,d) Viscous constants; (e,f) Characteristic times. The color code is denoted on the graphs, see also the inset in (a). The dashed lines present linear fits to the data.

### *3.6. Relaxation processes in alkane crystals – a possible molecular interpretation*

Our experimental data and their analysis revealed three distinct relaxation times in the rotator phases of linear alkanes. Their values differ by orders of magnitude, $t_1 \approx 0.45$ s and $t_2 \approx 8$–9 s for nonadecane and octacosane (very similar for both alkanes), while $t_3 = 137 \pm 36$ s for nonadecane and $206 \pm 11$ s for octacosane indicating longer $t_3$ for the longer alkane, see Fig. 7**e,f** and Table 1. These characteristic times do not vary significantly within the temperature range of rotator phase existence. Note that the elastic and viscous constants decrease noticeably when the temperature increase for $C_{19}$ (while for $C_{28}$ the observed temperature effect is negligible), however, because the decrease is similar, their ratios – the relaxation times became temperature independent in the frame of the experimental accuracy.

Therefore, in the following molecular interpretation of our data, we have to take into account and explain the most important experimental trends: (1) $G_0 \gtrsim G_1 \approx G_2 >> G_3$; (2) $t_3 >> t_2 >> t_1$; (3) $t_1$ and $t_2$ show no significant dependence on the alkane chain length, whereas $t_3$ increases with the alkane chain length.

The distinct values of the three relaxation times, $t_1$ to $t_3$, demonstrate that each of them corresponds to a different type of molecular

**Table 1**
Averaged values of the elastic and viscous constants, and their ratios – the characteristic times, determined from the analysis of stress-relaxation and creep-recovery data using the GKV3 model. The reported errors represent the standard deviations of the averaged values obtained from different experiments conducted under equivalent conditions, or, in the case of the characteristic times – for all temperatures examined for a given alkane.

| Alkane | | Nonadecane, $C_{19}$ | | Octacosane, $C_{28}$ | |
|---|---|---|---|---|---|
| Temperature | | 23°C | 28°C | 56°C | 60°C |
| Elastic constants GKV3 model, MPa | $G_0$ | 0.38 ± 0.04 | 0.25 ± 0.03 | 0.10 ± 0.03 | 0.10 ± 0.01 |
| | $G_1$ | 0.29 ± 0.06 | 0.18 ± 0.09 | 0.08 ± 0.02 | 0.11 ± 0.02 |
| | $G_2$ | 0.29 ± 0.08 | 0.19 ± 0.05 | 0.08 ± 0.02 | 0.09 ± 0.02 |
| | $G_3$ | 0.08 ± 0.02 | 0.07 ± 0.05 | 0.01 ± 0.002 | 0.015 ± 0.006 |
| Viscous constants GKV3 model, MPa.s | $\mu_1$ | 0.11 ± 0.03 | 0.08 ± 0.04 | 0.02 ± 0.01 | 0.05 ± 0.01 |
| | $\mu_2$ | 2.23 ± 0.85 | 1.48 ± 1.03 | 0.56 ± 0.31 | 0.92 ± 0.10 |
| | $\mu_3$ | 10.87 ± 4.32 | 8.62 ± 4.50 | 1.84 ± 0.94 | 3.10 ± 1.35 |
| Characteristic time | $t_1$ | 0.43 ± 0.05 | | 0.47 ± 0.06 | |
| | $t_2$ | 8.0 ± 0.8 | | 9.4 ± 0.5 | |
| | $t_3$ | 137 ± 36 | | 206 ± 11 | |

rearrangement in the deformed samples. On the other hand, the values of $G_i$ ($i = 1,2,3$) indicate three structurally different regions in the sheared samples. The highest elasticity $G_0$ should originate from the most ordered structural regions, viz. from the interior of the ordered lipid domains, see Fig. 8. The intermediate elasticities $G_1 \approx G_2$ should correspond to less ordered regions, while the much smaller value of $G_3$ could correspond to disordered regions. Based on the results from molecular dynamics simulations, performed previously, see Ref. [54], we propose that the region with intermediate elasticity, $G_1 \approx G_2$, is the boundary region at the surface of the ordered domains, in which many disordered *gauche* conformers in the terminal methyl and methylene groups are located. The softest material characterized by $G_3$ most probably corresponds to the layers of disordered alkane molecules, trapped upon freezing in between the neighboring ordered domains, see Fig. 8.

Based on the above assumptions, we can propose molecular explanations of the various constants and the underlying processes. The highest elastic constant, $G_0$, corresponds to purely elastic deformation of the ordered domains, e.g., a small change in the tilt of the ordered molecules in the planar structure of the sheared domains. These molecules could not relax in the time scale of our experiments under constantly applied deformation (as in the stress-relaxation experiments). For this reason, the elastic constant $G_0$ has no viscous and relaxation counterparts. Note that no crystalline phase is present in the studied samples, as all samples are in the rotator phase. The value of $G_0$ corresponds to molecules incorporated within the domains, where the number of defects is minimal or absent, whereas the other three values represent molecules located in regions with defects.

The relaxation processes characterized with $t_1$ and $t_2$ are related to the regions characterized with $G_1 \approx G_2$. Therefore, these processes should occur in the same structural regions, viz. in the boundary layers of the domains, but should involve different molecular dynamics which does not depend on the alkane chain-length. Based on these data, we propose that the shortest time $t_1$ should correspond to local rearrangements of the *gauche* conformers of the terminal methyl and methylene groups located in the boundary regions, thus relaxing rapidly the stress around these conformers. Note that (1) these local rearrangements do not depend on the alkane chain length, in agreement with the experimental observations, and (2) we measure the macro-response of the stressed material, which means that we detect the collective response of the rearrangement of multiple conformers in the boundary layers – that is why these collective effects take much longer time (a fraction of seconds) than the individual conformational changes of single molecules.

The relaxation time $t_2$ is significantly longer and should include some additional, slower rearrangement process in the same boundary regions. We propose that this process is rearrangement of the disordered molecules which are not included in the ordered domains, while being strongly entangled with the *gauche* conformers in the boundary layers of the ordered domains. These disordered molecules can relax part of the applied stress by rearranging some of their fragments perpendicularly to the domain walls – thus explaining why $t_2$ also does not depend significantly on the alkane chain length.

Finally, $t_3$ is much longer and exhibits a measurable dependence on the alkane chain length. Therefore, we propose that it reflects molecular displacements (translation and/or rotation) of the disordered molecules, located in the regions between the ordered domains. Such a displacement would take much longer time and will be slower for the larger molecules, because it involves translation and/or rotation of the entire molecule. This process could result also in relatively small in amplitude, reversible sliding of the neighboring domains with respect to each other (the disordered alkane molecules acting as a "lubricant" between the domains).

Note that the experimental data interpreted with the GKV and GM models correspond to small reversible deformations. Therefore, we do not consider larger in amplitude sliding of the neighboring domains

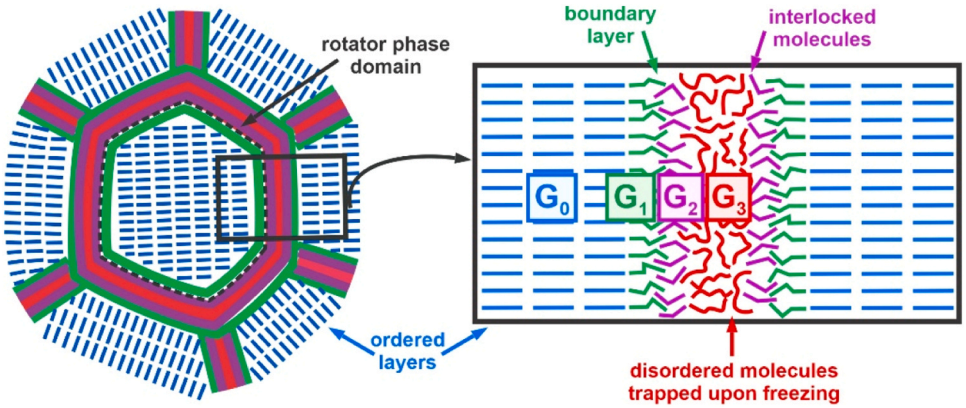


**Fig. 8.** Schematic representation of the molecular ordering in frozen alkane systems. Alkane molecules located within individual rotator phase domains (shown in blue) are arranged in well-ordered layers. Molecules at the surfaces of these ordered domains (shown in green) contain a high number of disordered *gauche* conformers. The layer of entangled, interlocked molecules is shown in purple, while alkane molecules trapped between the individual ordered domains and remaining disordered are shown in red. The elastic constants associated with the different regions are also indicated in the schematic.

which would change the relative positions of the neighboring domains, thus creating irreversible deformations like those observed at strains $\gamma > 3$-5%. Note that such interdomain sliding is observed in many polycrystalline materials, including nanocrystalline materials [55], alloys [56], ceramics [57] and even geological systems [58].

The above molecular interpretation is rather plausible, but it still remains speculative. Further dedicated experiments or molecular modelling of sheared alkane materials would be required to verify or to refine the molecular explanations proposed above.

## 4. Conclusions

The present study investigates the visco-elasto-plastic properties of the rotator phases of alkanes. A large series of creep-recovery and stress-relaxation rheological experiments are performed and the obtained results are analyzed using generalized rheological models. The absence of residue strain in the creep-recovery tests when the maximal deformation remained below ca. 5% and the establishment of a constant stress values at infinitely long time in the stress-relaxation tests performed in the linear visco-elastic region, show that one purely elastic element must be included in the model. Third-order models, i.e. containing three additional viscous and three additional elastic elements, were found to describe adequately all obtained experimental results in the linear regime.

Analysis of the experimental data, using the third-order generalized Maxwell (GM3) and Kelvin-Voigt (GKV3) models revealed the respective elastic and viscous contributions to the overall rheological response. We showed that obtaining accurate values for the first elastic constant associated with the first spring-dashpot element requires accounting for the complete strain *vs.* time profile in the stress-relaxation experiments. When the simpler assumption of a constant applied strain throughout the entire experiment was used to describe the data obtained after the initial few seconds, this elastic constant was systematically underestimated.

Based on the analysis of the sample structure, we concluded that the generalized Kelvin-Voigt model (GKV3) is adequate to describe the domain-structured bulk lipids. Therefore, we summarize in the conclusion only the results obtained with this model. The elastic constants had comparable values, e.g., $G_i \approx 0.07 - 0.25$ MPa for the rotator phase of nonadecane at 28°C using the GKV3 model, see Table 1. In contrast, the viscous constants varied within several orders of magnitude, between 0.08 and 8.62 MPa.s, reflecting also the wide span of the respective relaxation times – between ca. 0.5 and 200 s. Both the elastic and viscous constants were found to increase their values upon cooling within the temperature range of the rotator phase existence for nonadecane ($C_{19}$) in the temperature range between 21°C and 28°C. No significant dependence of the temperature was observed for octacosane ($C_{28}$) in the range of 56°C to 60°C. The relaxation times in both systems were practically independent of temperature in the frame of the experimental accuracy.

A plausible molecular interpretation of the observed relaxation processes is proposed. The values of the three characteristic relaxation times were determined to be: $t_1 \approx 0.45$ s, $t_2 \approx 8$–9 s, and $t_3 \approx 140$ – 200 s. We propose that the shortest time $t_1$ correspond to local rearrangements of the *gauche* conformers of the terminal methyl and methylene groups located in the boundary, less ordered regions of the alkane molecules included in the ordered domains. The relaxation time $t_2$ is proposed to reflect the rearrangement of the disordered molecules which are not included in the ordered domains, while being strongly entangled with the *gauche* conformers in the boundary layers of the ordered domains. Finally, $t_3$ is proposed to reflect molecular displacements (translation and/or rotation) of the disordered molecules, located in the regions between the ordered domains. The latter process could include also a relatively small in amplitude, reversible sliding of the neighboring domains with respect to each other (the disordered alkane molecules acting as a "lubricant" between the domains).

The present study serves as an example for the rheological investigation of the properties of crystalline and plastic materials composed of low-molecular weight solid phases, for which information in the literature is currently scarce. The approach demonstrated here can be applied to other polycrystalline materials to interpret their macroscopic rheological response and to extract characteristic relaxation times associated with their underlying structural and molecular dynamics.

## CRediT authorship contribution statement

**A. Todorova:** Investigation, Validation, Formal analysis, Visualization, Writing – original draft. **D. Cholakova:** Conceptualization, Methodology, Investigation, Validation, Formal analysis, Supervision, Visualization, Writing – original draft, review and editing. **N. Denkov:** Conceptualization, Writing – review & editing, Funding acquisition. **S. Tcholakova:** Conceptualization, Methodology, Formal analysis, Supervision, Writing – review & editing.

## Declaration of Competing Interest

The authors declare that they have no known competing financial interests or personal relationships that could have appeared to influence the work reported in this paper.

## Acknowledgements

The study was funded by the Bulgarian Ministry of Education and Science, under the National Research Program "VIHREN", project ROTA-Active (no. KP-06-DV-4/16.12.2019). We thank Ms. Krastina Tsvetkova for performing some preliminary experiments. S.T. acknowledges the support received from European Union-NextGenerationEU, through the National Recovery and Resilience Plan of the Republic of Bulgaria, project No BG-RRP-2.004–0008.

## Appendix A. Supporting information

Supplementary data associated with this article can be found in the online version at doi:10.1016/j.colsurfa.2026.140415.

## Data availability

Data will be made available on request.

## References

[1] A.G. Marangoni, S.E. McGauley, Relationship between crystallization behavior and structure in cocoa butter, Cryst. Growth Des. 3 (2003) 95–108, https://doi.org/10.1021/cg025580l.
[2] E.V. Gonçalves, S.C. da Silva Lannes, Chocolate rheology, Food Sci. Technol. 30 (2010) 845–851, https://doi.org/10.1590/S0101-20612010000400002.
[3] E.O. Afoakwa, A. Paterson, M. Fowler, J. Vieira, Effects of tempering and fat crystallisation behaviour on microstructure, mechanical properties and appearance in dark chocolate systems, J. Food Eng. 89 (2008) 128–136, https://doi.org/10.1016/j.jfoodeng.2008.04.021.
[4] G. Rizzo, J.E. Norton, I.T. Norton, Emulsifier effects on fat crystallization, Food Struct. 4 (2015) 27–33, https://doi.org/10.1016/j.foostr.2014.11.002.
[5] H. Zhong, K. Allen, S. Martini, Effect of lipid physical characteristics on the quality of baked products, Food Res. Int. 55 (2014) 239–246, https://doi.org/10.1016/j.foodres.2013.11.010.
[6] R.L.S. Viriato, M. de Souza Queirós, M.I.L. Neves, A.P.B. Ribeiro, M.L. Gigante, Improvement in the functionality of spreads based on milk fat by the addition of low melting triacylglycerols, Food Res. Int. 120 (2019) 432–440, https://doi.org/10.1016/j.foodres.2018.10.082.
[7] H.M. Ribeiro, J.A. Morais, G.M. Eccleston, Structure and rheology of semisolid o/w creams containing cetyl alcohol/non-ionic surfactant mixed emulsifier and different polymers, Int. J. Cosmet. Sci. 26 (2004) 47–59, https://doi.org/10.1111/j.0412-5463.2004.00190.x.
[8] B.J.D. Le Révérend, M.S. Taylor, I.T. Norton, Design and application of water-in-oil emulsions for use in lipstick formulations, Int. J. Cosmet. Sci. 33 (2011) 263–268, https://doi.org/10.1111/j.1468-2494.2010.00624.x.

[9] E.K. Park, K.W. Song, Rheological evaluation of petroleum jelly as a base material in ointment and cream formulations: Steady shear flow behavior, Arch. Pharm. Res. 33 (2010) 141–150, https://doi.org/10.1007/s12272-010-2236-4.

[10] J.W. Goodby, V. Görtz, S.J. Cowling, G. Mackenzie, P. Martin, D. Plusquellec, T. Benvegnu, P. Boullanger, D. Lafont, Y. Queneau, S. Chamberte, J. Fitremann, Thermotropic liquid crystalline glycolipids, Chem. Soc. Rev. 36 (2007) 1971–2032, https://doi.org/10.1039/B708458G.

[11] G. Blomquist, Structure and analysis of insect hydrocarbons, in: G.J. Blomquist, A.-G. Bagnères (Eds.), Insect Hydrocarbons: Biology, Biochemistry, and Chemical Ecology, Cambridge University Press, 2010, pp. 19–34, https://doi.org/10.1017/CBO9780511711909.

[12] K. Koch, B. Bhusan, H.-J. Ensikat, W. Barthlott, Self-healing of voids in the wax coating on plant surfaces, Philos. Trans. R. Soc. A 367 (2009) 1673–1688, https://doi.org/10.1098/rsta.2009.0015.

[13] F.M.A. Leyva-Gutierrez, T. Wang, Rotator phases of aliphatic aldehydes and implications for wax crystal growth in plants, Cryst. Growth Des. 23 (2023) 2351–2360, https://doi.org/10.1021/acs.cgd.2c01350.

[14] C. Gutiérrez-Blandón, A.A. Cuadri, P. Partal, A. Tenorio-Alfonso, C. Delgado-Sánchez, F.J. Navarro, Rheological aspects of solid-to-liquid phase transitions in paraffin wax/bitumen blends for thermal energy storage applications, Appl. Therm. Eng. 253 (2024) 123779, https://doi.org/10.1016/j.applthermaleng.2024.123779.

[15] G. Abdeali, A.R. Bahramian, A comprehensive review on rheological behavior of phase change materials fluids (slurry and emulsion): The way toward energy efficiency, J. Energy Storage 55 (2022) 105549, https://doi.org/10.1016/j.est.2022.105549.

[16] P. Zhang, Z.W. Ma, Z.Y. Bai, J. Ye, Rheological and energy transport characteristics of a phase change material slurry, Energy 106 (2016) 63–72, https://doi.org/10.1016/j.energy.2016.03.025.

[17] D. Cholakova, N. Denkov, Rotator phases in alkane systems: In bulk, surface layers and micro/nano-confinements, Adv. Colloid Interface Sci. 269 (2019) 7–42, https://doi.org/10.1016/j.cis.2019.04.001.

[18] E.B. Sirota, H.E. King Jr., D.M. Singer, H.H. Shao, Rotator phases of the normal alkanes: An x-ray scattering study, J. Chem. Phys. 98 (1993) 5809–5824, https://doi.org/10.1063/1.464874.

[19] H. Gang, O. Gang, H.H. Shao, X.Z. Wu, J. Patel, C.S. Hsu, M. Deutsch, B.M. Ocko, E. B. Sirota, Rotator phases and surface crystallization in α-eicosene, J. Phys. Chem. B 102 (1998) 2754–2758, https://doi.org/10.1021/jp980603l.

[20] E.B. Sirota, X.Z. Wu, The rotator phases of neat and hydrated 1-alcohols, J. Chem. Phys. 105 (1996) 7763–7773, https://doi.org/10.1063/1.472559.

[21] H. Zhang, S.M. Maguire, C. Nie, R.D. Priestley, P.J. Chirik, R.A. Register, E. C. Davidson, M.A. Webb, Rotator phases in chemically recyclable oligocyclobutanes, Chem. Mater. 36 (2024) 11596–11605, https://doi.org/10.1021/acs.chemmater.4c02576.

[22] A. Müller, An X-ray investigation of normal paraffins near their melting points, Proc. R. Soc. Lond. Ser. A 138 (1932) 514–530, https://doi.org/10.1098/rspa.1932.0200.

[23] E.B. Sirota, D.M. Singer, Phase transitions among the rotator phases of the normal alkanes, J. Chem. Phys. 101 (1994) 10873–10882, https://doi.org/10.1063/1.467837.

[24] E. Park, K. Song, Rheological evaluation of petroleum jelly as a base material in ointment and cream formulations: steady shear flow behaviour, Arch. Pharm. Res. 33 (2010) 141–150, https://doi.org/10.1007/s12272-010-2236-4.

[25] M. Makai, E. Csányi, Zs Németh, J. Pálinkás, I. Erős, Structure and drug release of lamellar liquid crystals containing glycerol, Int. J. Pharm. 256 (2003) 95–107, https://doi.org/10.1016/S0378-5173(03)00066-8.

[26] H. Peng, D. Zhong, X. Ling, Y. Li, Y. Wang, Q. Yu, X. She, Y. Li, Y. Ding, n-Alkanes phase change materials and their microencapsulation for thermal energy storage: A critical review, Energy Fuels 32 (2018) 7262–7293, https://doi.org/10.10.21/acs.energyfiels.8b01347.

[27] D. Cholakova, K. Tsvetkova, S. Tcholakova, N. Denkov, Rheological properties of rotator and crystalline phases of alkanes, Coll. Surf. A 634 (2022) 127926, https://doi.org/10.1016/j.colsurfa.2021.127926.

[28] M. Maroncelli, S.P. Qi, H.L. Strauss, R.G. Snyder, Nonplanar conformers and the phase behavior of solid n-alkanes, J. Am. Chem. Soc. 104 (1982) 6237–6247, https://doi.org/10.1021/ja00387a013.

[29] M.-C. Miguel, A. Vespignani, M. Zaiser, S. Zapperi, Dislocation jamming and Andrade creep, Phys. Rev. Lett. 89 (2002) 165501, https://doi.org/10.1103/PhysRevLett.89.165501.

[30] A.H. Cottrell, A microscopic theory of Andrade creep, Philos. Mag. Lett. 84 (2004) 685–689, https://doi.org/10.1080/09500830500036146.

[31] T.G. Langdon, Review: developments in the creep of materials over a period of more than a century, J. Mater. Sci. 60 (2025) 8158–18176, https://doi.org/10.1007/s10853-025-10922-6.

[32] E.N. da C. Andrade, On the viscous flow in metals, and allied phenomena, Proc. R. Soc. A 84 (1910) 1–12, https://doi.org/10.1098/rspa.1910.0050.

[33] E.N. da C. Andrade, The flow in metals under large constant stresses, Proc. R. Soc. A 90 (1914) 329–342, https://doi.org/10.1098/rspa.1914.0056.

[34] J. Weiss, D. Amitrano, Logarithmic versus Andrade's transient creep: Role of elastic stress re-distribution, Phys. Rev. Mat. 7 (2023) 033601, https://doi.org/10.1103/physrevmaterials.7.033601.

[35] J.H. Cho, I. Bischofberge, Yield precursor in primary creep of colloidal gels, Soft Matter 18 (2022) 7612, https://doi.org/10.1039/d2sm00884j.

[36] M. Siebenbürger, M. Ballauff, Th Voigtmann, Creep in colloidal glasses, Phys. Rev. Lett. 108 (2012) 255701, https://doi.org/10.1103/PhysRevLett.108.255701.

[37] M. Cloitre, R. Borrega, L. Leibler, Rheological aging and rejuvenation in microgel pastes, Phys. Rev. Lett. 85 (2000) 4819, https://doi.org/10.1103/PhysRevLett.85.4819.

[38] J. Rosti, J. Koivisto, L. Laurson, M.J. Alava, Fluctuations and scaling in creep deformation, Phys. Rev. Lett. 105 (2010) 100601, https://doi.org/10.1103/PhysRevLett.105.100601.

[39] J.P. Sethna, K.A. Dahmen, C.R. Myers, Crackling noise, Nature 410 (2001) 242–250, https://doi.org/10.1038/35065675.

[40] J.C. Dandrea, R. Lakes, Creep and creep recovery of cast aluminum alloys, Mech. Time-Depend. Mater. 13 (2009) 303–315, https://doi.org/10.1007/s11043-009-9089-6.

[41] N.L. Carter, S.H. Kirby, Transient creep and semibrittle behavior of crystalline rocks, Pure Appl. Geophys 116 (1978) 807–839, https://doi.org/10.1007/BF00876540.

[42] B.L. Farmer, R.K. Eby, Calculations of energies for self-diffusion in n-alkanes, Polymer 28 (1987) 86–92, https://doi.org/10.1016/0032-3861(87)90320-X.

[43] R.S. Narang, J.N. Sherwood, Self-diffusion in eicosane single crystals, Mol. Cryst. Liq. Cryst. 59 (1980) 167–174, https://doi.org/10.1080/00268948008071420.

[44] E. Morawetz, Enthalpies of vaporization of n-alkanes from C12 to C20, J. Chem. Thermodyn. 4 (1972) 139–144, https://doi.org/10.1016/S0021-9614(72)80018-1.

[45] H. Yamakawa, S. Matsukawa, H. Kurosu, S. Kuroki, I. Ando, Diffusional behavior of n-alkanes in the rotator phase as studied by pulse field-gradient spin-echo $^{1}$H NMR method, J. Chem. Phys. 111 (1999) 7110, https://doi.org/10.1063/1.480003.

[46] R.G. Ricarte, S. Shanbhag, A tutorial review of linear rheology for polymer chemists: basics and best practices for covalent adaptable networks, Polym. Chem. 15 (2024) 815–846, https://doi.org/10.1039/d3py01367g.

[47] R.O. Ebewele, Polymer Science and Technology. Chapter 14 – Polymer viscoelasticity, CRC Press, Boca Raton, New York, 2000.

[48] K.P. Menard, K. Peter, Dynamic mechanical analysis: A practical introduction, CRC Press, Washington DC, 1999.

[49] D. Gutierrez-Lemini, Engineering Viscoelasticity, Springer, New York, 2014.

[50] A. Serra-Aguila, J.M. Puigoriol-Forcada, G. Reyes, J. Menacho, Viscoelastic models revisited: characteristics and interconversion formulas for generalized Kelvin-Voigt and Maxwell models, Acta Mech. Sin. 35 (2019) 1191–1209, https://doi.org/10.1007/s10409-019-00895-6.

[51] A. Chakrabarti, J.K. Ghosh, AIC, BIC and recent advances in model selection, Philos. Stat. 7 (2011) 583–605, https://doi.org/10.1016/B978-0-444-51862-0.50018-6.

[52] T.G. Mezger, The rheology handbook 2nd Ed, Hannover, Germany, 2006.

[53] K. Golemanov, S. Tcholakova, N. Denkov, E. Pelan, S.D. Stoyanov, Surface shear rheology of saponin adsorption layers, Langmuir 28 (2012) 12071–12084, https://doi.org/10.1021/la302150j.

[54] S. Iliev, S. Tsibranska, A. Ivanova, S. Tcholakova, N. Denkov, Computational assessment of hexadecane freezing by equilibrium atomistic molecular dynamics simulations, J. Colloid Interface Sci. 638 (2023) 743–757, https://doi.org/10.1016/j.jcis.2023.01.126.

[55] A.-K. Maier, D. Mari, I. Tkalcec, R. Schaller, Theoretical modelling of grain boundary anelastic relaxations, Acta Mater. 74 (2014) 132–140, https://doi.org/10.1016/j.actamat.2014.04.016.

[56] D.R. Mosher, R. Raj, Use of the internal friction technique to measure rates of grain boundary sliding, Acta Met. 22 (1974) 1469–1474, https://doi.org/10.1016/0001-6160(74)90108-4.

[57] S. Mototsugu, M. Hiroyuki, H. Mikichika, Stress relaxation of polycrystalline ceramics with grain-boundary sliding and grain interlocking, J. Am. Ceram. Soc. 82 (1999) 169–177, https://doi.org/10.1111/j.1151-2916.1999.tb01737.x.

[58] T.F. Fliervoet, S.H. White, D. Martyn R, Evidence for dominant grain-boundary sliding deformation in greenschist-and-amphibolite-grade polymineralic ultramylonites from the Redbank Deformed Zone, Central Australia, J. Struct. Geol. 19 (1997) 1495–1520, https://doi.org/10.1016/S0191-8141(97)00076-X.